Earth and Planetary Science Letters 461 (2017) 46–53

Contents lists available at ScienceDirect

Earth and Planetary Science Letters

www.elsevier.com/locate/epsl

Explicitly modelled deep-time tidal dissipation and its implication for Lunar history

J.A.M. Green [a,*], M. Huber [b], D. Waltham [c], J. Buzan [b], M. Wells [d]

[a] School of Ocean Sciences, Bangor University, Menai Bridge, United Kingdom
[b] Department of the Earth Sciences, The University of New Hampshire, Durham, NH, USA
[c] Department of Earth Sciences, Royal Holloway University of London, Egham, United Kingdom
[d] Department of Earth Science & Engineering, Imperial College London, London, United Kingdom

ARTICLE INFO

Article history:
Received 7 January 2016
Received in revised form 20 December 2016
Accepted 23 December 2016
Available online 6 January 2017
Editor: M. Frank

Keywords:
tides
tidal drag
Earth–Moon evolution
Mesozoic–Cenozoic
numerical tidal model

ABSTRACT

Dissipation of tidal energy causes the Moon to recede from the Earth. The currently measured rate of recession implies that the age of the Lunar orbit is 1500 My old, but the Moon is known to be 4500 My old. Consequently, it has been proposed that tidal energy dissipation was weaker in the Earth's past, but explicit numerical calculations are missing for such long time intervals. Here, for the first time, numerical tidal model simulations linked to climate model output are conducted for a range of paleogeographic configurations over the last 252 My. We find that the present is a poor guide to the past in terms of tidal dissipation: the total dissipation rates for most of the past 252 My were far below present levels. This allows us to quantify the reduced tidal dissipation rates over the most resent fraction of lunar history, and the lower dissipation allows refinement of orbitally-derived age models by inserting a complete additional precession cycle.

1. Introduction

Tidally induced energy dissipation in the earth and ocean gradually slows the Earth's rotation rate, changes Earth and lunar orbital parameters, and increases the Earth–Moon separation (Darwin, 1899; Munk, 1968). A long-standing conundrum exists in the evolution of the Earth–Moon system relating to the present recession rate of the moon and its age: if present day observed dissipation rates are representative of the past, the moon must be younger than 1500 Ma (Hansen, 1982; Sonett, 1996). This does not fit the age model of the solar system, putting the age of the moon around 4500 Ma (Hansen, 1982; Sonett, 1996; Walker and Zahnle, 1986; Canup and Asphaug, 2001; Waltham, 2004), and the possibility that the tidal dissipation rates have changed significantly over long time periods has been proposed (Hansen, 1982; Ooe, 1989; Poliakov, 2005; Green and Huber, 2013; Williams et al., 2014). A weaker tidal dissipation must be associated with a lower recession rate of the moon. Consequently, it can be argued that prolonged periods of weak tidal dissipation must have existed in the past (Webb, 1982; Bills and Ray, 1999; Williams, 2000). There is support for this in the literature using quite coarse resolution simulations driven by highly stylized, rather than historically accurate, boundary conditions (Munk, 1968; Kagan and Sundermann, 1996). However, with the present knowledge of the sensitivity of tidal models to resolution and boundary conditions, e.g., the oceans density structure (Egbert et al., 2004), the results of prior work should be revisited with state-of-the-art knowledge and numerical tools.

It was recently shown through numerical tidal model simulations with higher resolution than in previous studies that the tidal dissipation during the early Eocene (50 Ma) was just under half of that at present (Green and Huber, 2013). This is in stark contrast to the Last Glacial Maximum (LGM, around 20 ka) when simulated tidal dissipation rates were significantly higher than at present due to changes in the resonant properties of the ocean (Green, 2010; Wilmes and Green, 2014; Schmittner et al., 2015). However, the surprisingly large tides during the LGM are due to a quite specific combination of continental scale bathymetry and low sea-level, in which the Atlantic is close to resonance when the continental shelf seas were exposed due to the formation of extensive continental ice sheets (Platzman et al., 1981; Egbert et al., 2004; Green, 2010). It is therefore reasonable to assume — and proxies support this — that the Earth has only experienced very large tides during the glacial cycles over the last 1–2 Ma and that the rates have been lower than at present during the Cenozoic (Palike and Shackleton, 2000; Lourens and Brumsack, 2001; Lourens et al., 2001). Such (generally) low tidal dissipation rates

* Corresponding author.
E-mail address: m.green@bangor.ac.uk (J.A.M. Green).

http://dx.doi.org/10.1016/j.epsl.2016.12.038

may have led to reduced levels of ocean mixing, with potential consequences for the large scale ocean circulation, including the Meridional Overturning Circulation (Munk, 1966; Wunsch and Ferrari, 2004).

The tidally induced lunar recession and increased day length also act to reduce the precession rate of Earth's axis and, as a result, produce falling rates of climatic precession and obliquity oscillation through time (Berger et al., 1992). As a direct consequence, cyclostratigraphy may be severely compromised because many important Milankovitch cycle periods are directly affected by the Earth–Moon separation. Nevertheless, Milankovitch frequencies have been estimated assuming either a constant lunar-recession rate or a constant tidal dissipation rate (Berger et al., 1992; Laskar et al., 2004). Based on the literature related to tidal evolution mentioned above, neither assumption is valid. For example, it was recently suggested that the tidal dissipation between 11.5–12.3 Ma was either at least 90% of the Present Day (PD) rate or 40% of the present rate, with the lower estimate obtained by shifting the precession a whole cycle (Zeeden et al., 2014). Constraining the tidal dissipation rates on geological time scales is consequently important. Investigating the tidal dynamics for select time slices over the Cenozoic era will shed light on the changes of tidal dissipation and hence on Earth–Moon system evolution.

Our aim in this paper is to answer the basic question: when considering the past, should our null hypothesis be that tidal dissipation was near modern values (the most common approach), much higher (suggested by LGM), or much lower (such as found for the Eocene)? We use the same tidal model as Green and Huber (2013), and we present results from simulations of the tidal dynamics for the PD, LGM (21 ka, Green, 2010), Pliocene (3 Ma), Miocene (25 Ma), Eocene (50 Ma, Green and Huber, 2013), Cretaceous (116 Ma, Wells et al., 2010), and for the Permian–Triassic (252 Ma). We explore dissipation changes across a wide cross-section of ocean states and palegeographic configurations, from the nearly modern to a world with one global ocean basin, and we investigate sensitivity to substantial imposed changes in ocean stratification. Consequently, this encompasses the likely range of continental and paleoclimate configurations over much of Earth's history.

2. Methods

2.1. Tidal modelling

The simulations of the global tides were done using the Oregon State University Tidal Inversion Software (OTIS, Egbert et al., 1994). OTIS has been used in several previous investigations to simulate global tides in the past and present oceans (Egbert et al., 2004; Green, 2010; Green and Huber, 2013; Wilmes and Green, 2014). It provides a numerical solution to the linearized shallow water equations,

$$\frac{\partial \mathbf{U}}{\partial t} + \mathbf{f} \times \mathbf{U} = -gH\nabla(\eta - \eta_{SAL} - \eta_{EQ}) - \mathbf{F} \quad (1)$$

$$\frac{\partial \eta}{\partial t} - \nabla \cdot \mathbf{U} = 0 \quad (2)$$

Here $U = uH$ is the volume transport given by the velocity u multiplied by the water depth H, f is the Coriolis parameter, η the tidal elevation, η_{SAL} the self-attraction and loading elevation, η_{EQ} the equilibrium tidal elevation, and $\mathbf{F}$ the dissipative term. Self-attraction and loading was introduced by doing 5 iterations following the methodology in Egbert et al. (2004). The dissipative term is split into two parts: $\mathbf{F} = \mathbf{F}_B + \mathbf{F}_W$. The first of these represents bed friction and is written as

$$\mathbf{F}_B = C_d \mathbf{u}|\mathbf{u}| \quad (3)$$

where C_d is a drag coefficient, and $\mathbf{u}$ is the total velocity vector for all the tidal constituents. We used $C_d = 0.003$ in the simulations described below, but for all time slices simulations were done where C_d was increased or decreased by a factor 3 to estimate the sensitivity of the model to bed roughness. This only introduced minor changes in the results (within a few percent of the control), and we opted to use the value which provided the best fir to observations for the present. The second part of the dissipative term, $\mathbf{F}_w = C\mathbf{U}$, is a vector describing energy losses due to tidal conversion. The conversion coefficient C is here defined as Green and Huber (2013)

$$C(x, y) = \gamma \frac{(\nabla H)^2 N_b \bar{N}}{8\pi\omega} \quad (4)$$

in which $\gamma = 100$ is a scaling factor, N_b is the buoyancy frequency at the sea-bed (taken from coupled climate model outputs), $\bar{N}$ is the vertical average of the buoyancy frequency, and ω is the frequency of the tidal constituent under evaluation. We did simulations with varying scaling factors (with $50 < \gamma < 200$) to cover the possible ranges of N, with only minor quantitative changes to the overall dissipation rates. This means that errors and uncertainties in the estimates of the buoyancy frequency from the climate model simulations will only change the quantitative results less than 10%.

The PD bathymetry is a combination of v.14 of the Smith and Sandwell database (Smith and Sandwell, 1997) with data for the Arctic (Jakobsson et al., 2012), northwards of 79°N, and Antarctic (Padman et al., 2002), southwards of 79°S. All data were then averaged to 1/4° in both latitude and longitude.

The PD control simulation is compared to the TPXO8 database, an inverse tidal solution for both elevation and velocity based on satellite altimetry and the shallow water equations (see Egbert and Erofeeva, 2002, and http://volkov.oce.orst.edu/tides/tpxo8_atlas.html for details). The root-mean-square (RMS) difference between the modelled and observed elevations is computed, along with the percentage of sea surface elevation variance captured, given by $V = 100[1 - (S/RMS)^2]$, where RMS is the RMS discrepancy between the modelled elevations and the TPXO elevations, and S is the RMS of the TPXO elevations.

The tidal dissipation, D, is computed using (Egbert and Ray, 2001):

$$D = W - \nabla \cdot P \quad (5)$$

in which W is the work done by the tide-producing force and P is the energy flux. They are defined as

$$W = g\rho\langle \mathbf{U} \cdot \nabla(\eta_{SAL} + \eta_{EQ}) \rangle \quad (6)$$

$$P = g\rho\langle \eta \mathbf{U} \rangle \quad (7)$$

in which the angular brackets mark time-averages. When we discuss the accuracy and the energy dissipation rates we use a cutoff between deep and shallow water at 1000 m depth.

2.2. Earth–Moon separation

The tidal dissipation rate, D, should be (Murray and Dermott, 2010)

$$D = 0.5 m' n a (\Omega - n) \frac{\partial a}{\partial t} \quad (8)$$

where $m' = mM/(m + M)$, m is Moon-mass, M is Earth-mass, a is the Earth–Moon separation, Ω is the Earth's rotation rate and n is the lunar mean motion. The next step is to note that lunar recession is well approximated using (Lambeck, 1980; Bills and Ray, 1999; Waltham, 2015)

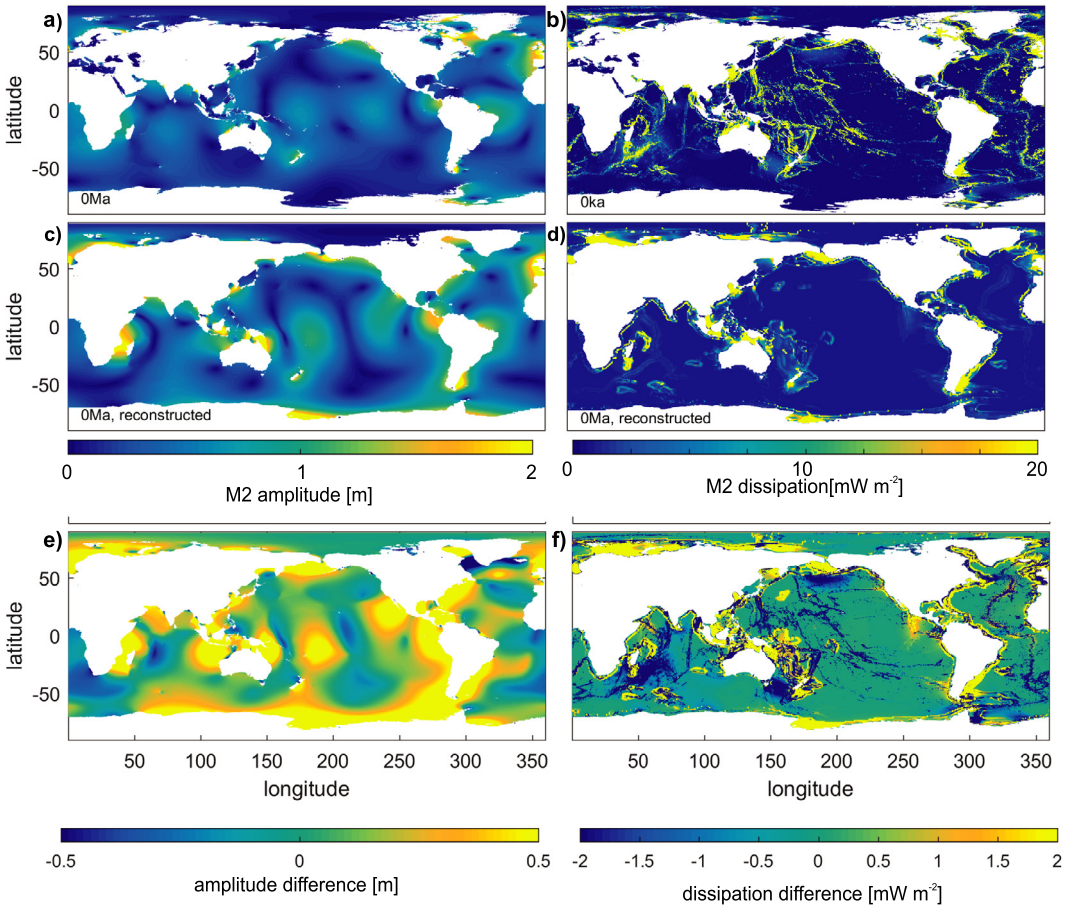

Fig. 1. Modelled M_2 tidal amplitudes for the PD (a) and the PD reconstruction (c), and the difference between the two panels (e). Panels b, d, and f show the associated tidal dissipation rates.

$$\frac{\partial a}{\partial t} = f a^{-5.5} \tag{9}$$

where the tidal drag factor

$$f = 3\frac{k_2 m}{Q\,M} R^5 \sqrt{\mu} \tag{10}$$

In which k_2 is Earth's Love number, Q is the tidal quality factor, R is Earth's radius whilst, from Kepler's 3rd Law

$$\mu = G(m + M) = n^2 a^3 \tag{11}$$

Combining Eqs. (8)–(11) yields

$$f = \frac{2Da^6}{m'\sqrt{\mu}(\Omega - n)} \tag{12}$$

Note that the tidal dissipation rates calculated in Table 1 assumed the present-day day-length and Earth–Moon separation. All terms in Eq. (12), except D, were therefore constant so $f/f_{PD} = D/D_{PD}$. This is a reasonable approximation as day-lengths and Earth–Moon separation only change by a few percent over the time-range considered (e.g., Waltham, 2015).

3. Results

3.1. Tidal evolution

Simulations were carried out with the M_2, S_2, K_1, and O_1 tidal constituents included (representing the principle lunar and solar semidiurnal constituents, and constituents representing the diurnal luni-solar and lunar declinations, respectively). Here, we limit our discussion to M_2 as changes in the other constituents are similar to those in M_2 but smaller in magnitude (see the discussion below). Building on prior work we aim to create a time history of paleodissipation by filling in new simulations of the Permian–Triassic, Cretaceous, Miocene, and Pliocene. To further understand the sensitivity of our results to our methodological choices and to establish their robustness we conducted a degraded PD sensitivity simulation, in which we used a bathymetric database for the present ocean derived using the same geophysical principals and methods as our paleo-bathymetries (see Matthews et al., 2015). This simulation showed a total M_2 dissipation of some 4.5 TW, of which 1 TW dissipated in deep waters (Table 1 and Fig. 1). This is within a factor 2 of our values using present day observed bathymetry (2.8 TW in total and 0.9 TW in the deep, respectively) and leads us to conclude that we most likely overestimate the dissipation rates in our paleo-simulations due to a lack of abyssal topography (see Egbert et al., 2004, for a similar discussion). Our integrated values presented below are therefore probably on the high side in terms of absolute magnitude but we concentrate on relative changes in this study. The robustness of our results in our sensitivity simulation also gives us confidence in our bathymetric databases. In the rest of this analysis we generally present results normalized by the reconstructed PD dissipation values in order to show only relative changes with respect to the modern degraded simulation. The one exception is the LGM study, which is normalized by the undegraded PD simulations since modern observed bathymetry was used in this simulation. In the following we refer the reader to Fig. 1 and Table 1 for the PD results, and Figs. 2–3 for palaeo-tidal M_2 amplitudes and dissipation rates, respectively.

Table 1
The integrated tidal dissipation rates (in TW) for the M_2 constituent for the global ("total") and abyssal ("deep", i.e., deeper than 1000 m) ocean. The relative rate for PD is normalised with the PD reconstructed rate, whereas the relative LGM rate is normalised with the PD rate (see Fig. 1 and the text for a discussion).

Period, age	Absolute total	Deep	Relative total	Comment/source
PD	2.8	0.9	0.62	Green and Huber (2013)
PD reconstructed	4.5	1.0	1	PD with reconstructed bathymetry
LGM 0.021 Ma	4.0	1.5	1.42	Wilmes and Green (2014), relative to PD

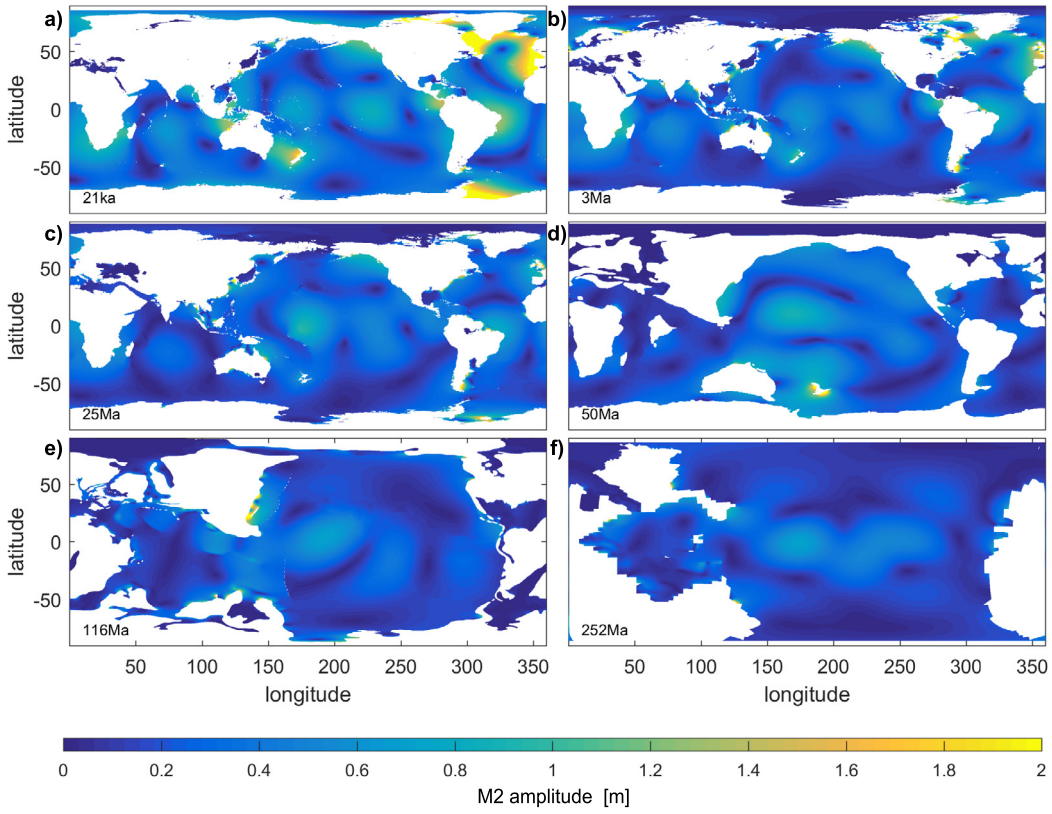

Fig. 2. Shown are the M_2 tidal amplitudes for the LGM (a), Pliocene (b), Miocene (c), Eocene (d), Cretaceous (e) and Permian–Triassic (f).

Table 2 and Fig. 4 summarise the globally integrated relative dissipation rates.

The Pliocene simulations exhibit a reduced amplitude and subsequent dissipation rate (53%) compared to the degraded PD tides, but with a very similar distribution (Figs. 2b and 3b). This is due to sea-level being some 25 m higher than at present during this period and is consistent with previously reported simulations with extreme sea level rise (SLR; Green and Huber, 2013). The dynamical explanation is that the large SLR cause global dissipation rates to drop below present because the near-resonant North Atlantic experiences decreased dissipation rates with SLR due to larger shelf seas (Green, 2010).

Simulated Miocene tides resemble the modelled degraded PD tides to some extent, but they are generally weaker than at present (Figs. 2c and 3c). The globally integrated dissipation rate for the Miocene is 2.2 TW, or 50% of the degraded model present rate. These changes are mainly explained by the Atlantic being narrower during the Miocene than the PD. The North Atlantic is therefore no longer near resonance for the semi-diurnal tide, which reduces the simulated Miocene tidal amplitudes. The vertical stratification in our Miocene simulations was stronger than at present due to different ocean gateway configurations and the lack of North Atlantic Deepwater formation, which leads to a more stably stratified ocean (Herold et al., 2012). This enhances the tidal conversion in the abyssal ocean, and as a consequence there is more energy being lost in the deep ocean in the Miocene case than at present. Further support comes from sensitivity simulations which used enhanced or reduced stratifications based on the ratio between the averaged PD and Miocene buoyancy frequencies (not shown). In these runs a combination of Miocene stratification and PD bathymetry leads to a reduced global and enhanced abyssal dissipation compared to the Miocene control simulation. The opposite holds when using PD stratification with the Miocene bathymetry.

We have carried out a set of climate model sensitivity runs to complement the earlier Eocene simulation (see Table 2). These used a tidally driven diffusivity parameterization (Green and Huber, 2013) but with atmospheric CO_2 concentrations of 240 ppm, 560 ppm, and 1120 ppm. Further runs with Drake Passage or the Tasman Gateway open were also conducted, using 560 ppm CO_2 (changes in CO_2 may affect tides by modifying the stratification-dependent tidal conversion rate). These simulations were carried out to bound the sensitivity of the Eocene results to likely changes in surface climate and ocean gateway configuration that are thought to have altered ocean stratification, a key parameter in tidal studies. There are only small changes in the tidal conversion rates between these runs and the Eocene control (see our Table 2, Figs. 2d and 3, and Green and Huber, 2013), indicating that the ocean state and tidal dissipation are convergent.

The new model results for the Cretaceous show a somewhat energetic ocean, dissipating nearly as much energy as the Miocene (Figs. 2e and 3e). The reason for this quite large simulated dissipation rate lies in the rifting of Gondwanaland, which generated

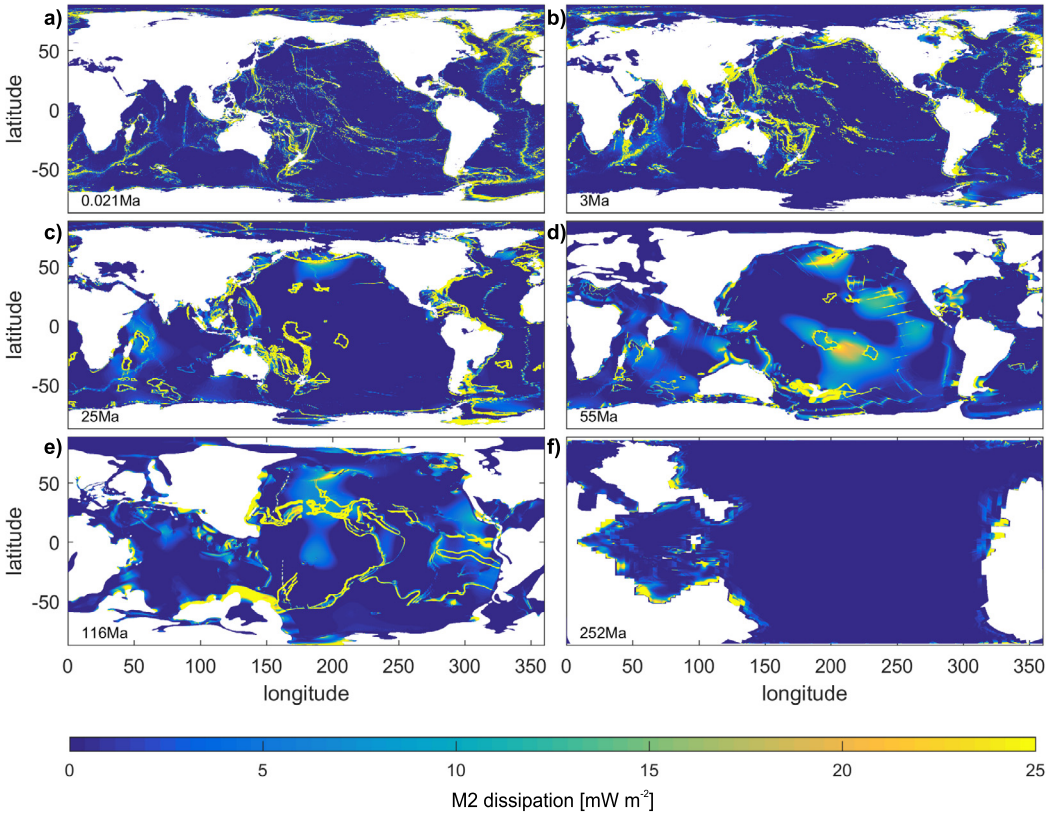

Fig. 3. As in Fig. 2, but showing the modelled *absolute* tidal dissipation rates.

Table 2
The integrated absolute tidal dissipation rates (in TW) for the M_2 constituent for the palaeo-simulations. Shown are again data for the global ("total") and abyssal ("deep", i.e., deeper than 1000 m) ocean. The relative rate is normalised with the total rate for the reconstructed PD simulation.

Period, age	Absolute total	Deep	Relative total	Comment/source
Pliocene 3 Ma	2.4	0.6	0.53	
Miocene 25 Ma	2.2	0.6	0.49	
	1.9	1.7	0.43	PD bathymetry, Miocene stratification
	3.3	<0.1	0.73	PD stratification, Miocene bathymetry
Eocene 50 Ma	1.4	1.2	0.32	Green and Huber (2013)
	1.4	1.2	0.32	$CO_2 = 240$ ppm
	1.4	1.2	0.32	$CO_2 = 560$ ppm
	1.4	1.2	0.32	$CO_2 = 1120$ ppm
	1.4	1.2	0.32	Tasman Gateway open
	1.4	1.2	0.32	Drake Passage open
Cretaceous 116 Ma	2.1	1.3	0.47	
	2.0	1.5	0.44	Tidal conversion × 2
	2.1	1.0	0.47	Tidal conversion × 0.5
Permian–Triassic 252 Ma	0.9	0.1	0.2	
	0.8	0.2	0.18	Tidal conversion × 2

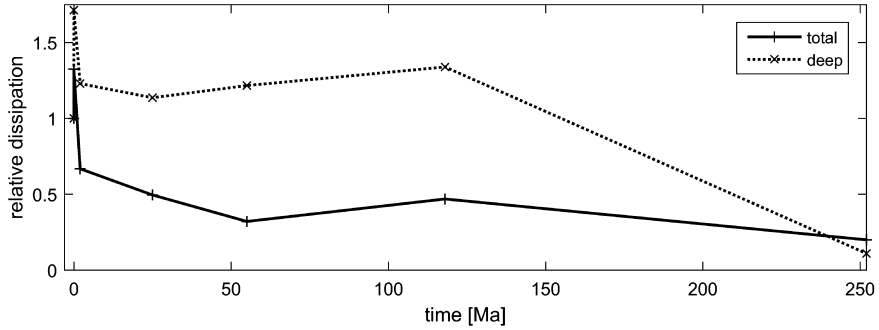

Fig. 4. Shown are the *relative* dissipation rates, normalized with the results from the PD sensitivity run. This confirms that total rates have been lower over the last 252 Ma, but that the abyssal rates have generally been larger than today.

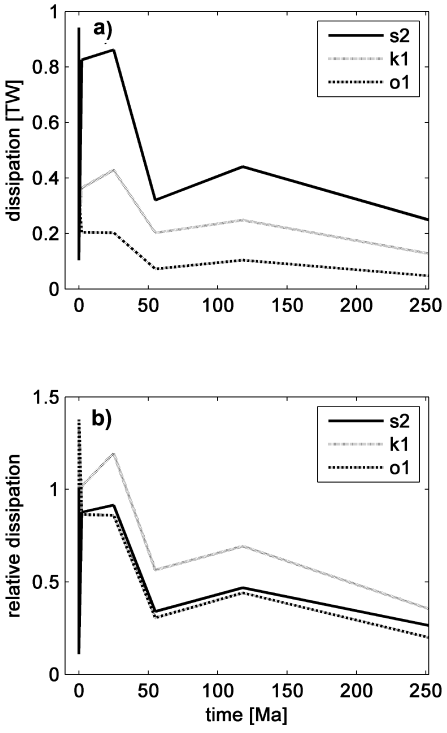

Fig. 5. As in Fig. 4 but for the S_2, K_1, and O_1 constituents.

extensive new coastlines and a corresponding increase in the surface area of shallow shelf seas (Wells et al., 2010). The Cretaceous shelf seas in the model cover an area more than three times larger than that at present. These very vast shallow areas, together with a strong vertical stratification (the average buoyancy frequency used in the model is nearly twice that at Present, e.g., Zhou et al., 2012; Poulsen and Zhou, 2013; Domeier, 2016), lead to relatively large dissipation rates overall. A large fraction of this energy, about 62%, ends up in the deep ocean in the simulations. The lack of knowledge about the abyssal topography for this period can be compensated for by varying the tidal conversion coefficient as a sensitivity parameter. Using factors of 0.5 and 2 above the already doubled value compared to PD discussed above to provide sensitivity estimates, we still obtain much less than modern dissipation in the Cretaceous case (Table 2) and are confident in our conclusions.

The Permian–Triassic (PT) simulations show very weak tides with a total dissipation of about 1 TW (22% of degraded PD; Figs. 2f and 3f) — 10% of which dissipates in the deep ocean. These results are readily understandable, as the large recent dissipation rates are an effect of complex bathymetry and local resonances in smaller basins between continents and such features were absent during the PT (see Muller et al., 2016 for a discussion). Simulations of a PD water world show similar behaviour, albeit with even weaker tides than we find here, because with less topographic variations we approach the theoretical equilibrium tide (Arbic et al., 2009). The PT simulation with a doubled tidal conversion coefficient, representing unaccounted for topographic roughness (see Table 2), showed a 45% increase in the abyssal rates but a 9% reduction in total dissipation. This again puts us on the safe side with our conclusions because we probably overestimate the dissipation slightly in the PT control run.

The horizontally integrated dissipation rates for the other constituents, S_2, K_1 and O_1, are shown in Fig. 5. It is evident from Fig. 5 that the behaviour of these constituents mimic that of the M_2 tide and that the M_2 is a good representation of the global tidal dissipation. It is possible that basins may become resonant for the diurnal constituents (although this has not been spotted in our simulations), but they are by their very nature less energetic than M_2. The conversion of energy in the diurnal constituents is also more restricted due to the critical latitude being only 30° (see Falahat and Nycander, 2015, for a discussion).

3.2. Consequences for the Earth–Moon system

The lower-than-modern tidal dissipation rates simulated through the Cenozoic and Mesozoic shows that the lunar recession rate was probably smaller than otherwise predicted in the past. The questions raised are i) by how much? and ii) how did this impact on the lunar distance? Using the recession model in Section 2.2, we show that the relative tidal dissipations in Tables 1–2 are also the relative tidal-drag ratios. It is notable that all but the most recent ratios are significantly below unity. This is consistent, however, with the observation that the long-term mean drag must be around $f/f_{PD} = 0.33 \pm 0.03$ if the Moon-forming collision occurred at 4500 ± 50 Ma (Waltham, 2015). The implications of both the ancient origin of our Moon, and the tidal-dissipation modelling in this paper, are that present day tidal dissipation is anomalously high. Given the results in Table 2, the typical tidal drag over the last 250 Ma is $f/f_{PD} = 0.63 \pm 0.16$ (1 standard error). Using this result in Eq. (9) then yields the Earth–Moon separation history shown in Fig. 6. For comparison, Fig. 6 also shows the results of full numerical modelling by Laskar et al. (2004) along with the results of using Eq. (9) assuming $f/f_{PD} = 1$. Note that Laskar et al. (2004) assumed that tidal lag (which is closely related to tidal drag) did not vary from the present day value in the past.

4. Discussion

It is obvious, especially from the sensitivity tidal simulations, that the lunar distance would have been changing more slowly in the past than would be predicted assuming modern dissipation rates. It has been suggested that the average recession rate from the late Neoproterozoic (620 Ma) to PD is 2.17 cm yr^{-1}, and that the recession rate during the Proterozoic (2450–620 Ma) cannot have exceeded of 1.24 cm yr^{-1} (Williams, 2000). Both of these statements are supported here, and we suggest that the rates may even have been lower. Furthermore, because the recession rate is proportional to tidal-lag (Laskar et al., 2004), and we have shown that the recession rate is proportional to dissipation, the tidal-lag must have an uncertainty of a factor of 2 or more. This confirms, using a very different approach, suggestions about uncertainty in Milankovitch periods and cyclostratigraphy (Waltham, 2015). Furthermore, sensitivity simulations (not shown) with sea-level being 80 m higher or lower in each time slice did not significantly change the results, except for PD, when large shelf seas are present and allowed to dry out or flood further (see Green and Huber, 2013, for a discussion). From these results it also appears that Earth is near a tidal maximum at present, although full glacial conditions enhance dissipation by a further 42%.

Given that most of the Phanerozoic has been spent with either much warmer climate than modern conditions (with weaker stratification) or continents more widely spaced and oceans out of resonance, it is now clear that the modern situation is a poor guide to the past as suggested by Hansen (1982). A more accurate null hypothesis is to assume that overall tidal dissipation was typically around 50% of modern values, although subject to significant variation. Interestingly, this result compares well with independent estimates from rhythmites (Williams, 2000; Coughenour et al., 2013). The similarity of the results obtained here with prior modelling work utilizing much simpler physical formulations of dissipation and much cruder representations of varying boundary conditions (Hansen, 1982; Webb, 1982; Kagan and Sundermann, 1996; Poliakov, 2005) is also noteworthy. This similarity confirms that the

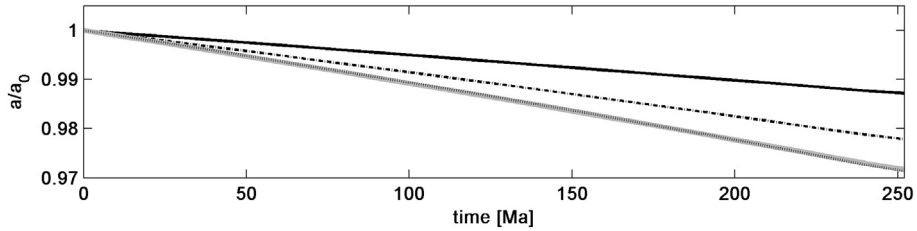

Fig. 6. Earth–Moon separation through time from Equations (9)–(12). The solid and dashed–dotted black lines show the range assuming the tidal-dissipation range of this paper. The solid grey line shows lunar-recession assuming that tidal-dissipation equalled the present day dissipation in the past, whereas the black dotted line shows the lunar-separation history predicted by the full numerical model from Laskar et al. (2004). Note that the Laskar model is virtually identical to our curve, assuming PD tidal drag, but that the lower mean-drag shown in this paper gives a reduced separation in the past.

physics of tidal dissipation and the bulk variables that cause it to vary are robust and constrainable.

Tides are of course not the only process affecting orbital parameters, and the different plate tectonic configurations over the past 252 Ma may have altered the dynamical ellipticity, adding to the changes discussed here. This is, as stated in the introduction, an investigation into how the tides may have changed over long geological time scales and the possible contributions from the tides. Other mechanisms are left to other investigations. The ability to put significant bounds on tidal dissipation through time has substantial implications, especially for improving knowledge of Earth's precession parameters through time. The combination of tidal dissipation and the dynamical ellipticity (or so-called precession constant) is crucial for gaining more accurate solutions to Earth's precession and obliquity behaviours on long time scales. The importance of dissipation and dynamical ellipticity to these precession parameters allows them to be inferred by inverting interference patterns between obliquity and precession bands derived from long paleoclimate time-series and comparison with orbital calculations. From these calculations constraints on the summed behaviour of tidal dissipation and dynamical ellipticity can be gained, although the solutions tend to be non-unique. It has been suggested that a tidal dissipation value of approximately half of the modern rate characterized the past 3 Ma well (Lourens and Brumsack, 2001). This is in agreement with our results, but that study did not explore sensitivity to dynamical ellipticity. Significant uncertainty remains on this issue; other studies have reached the conclusion that tidal dissipation may have been higher (Palike and Shackleton, 2000), whereas more recent work, extending these methods further back to the early Miocene, show as much evidence for low (30–50% of modern) values of dissipation as they do higher (by 20%) (Husing et al., 2007; Zeeden et al., 2014). What is clear however, is that integrating these various approaches, including explicit modelling of tidal dissipation, will help resolve important paleoclimate and geophysical enigmas and improve cyclostratigraphic age models. For example, our low dissipation rates in Fig. 3 agree with the lower range of dissipation values from Zeeden et al. (2014) for 11.5–12.3 Ma if we shift the orbitally derived time scale for this interval by a whole precession cycle as compared to using a modern value. Explicitly modelling tidal dissipation will enable one of the two key free parameters in precession and obliquity calculations to be constrained which will enable a better understanding of the factors determining dynamical ellipticity.

The weaker tidally induced ocean mixing during the Phanerozoic may also have influenced the Meridional Overturning Circulation, with potential consequences for climate. Green and Huber (2013) used modelled stratification for the Eocene, whereas Schmittner et al. (2015) simulated the LGM with modelled stratification. Both investigations highlight local changes in dissipation, but the overall rates stayed within the range given by our sensitivity simulations. However, the percentage of upwelling from the deep was sometimes greater than at Present, and the consequences for the ocean circulation of reduced (tidally driven) mixing is complex and needs further investigation.

5. Conclusions

Results from an established numerical tidal model suggest that the tidal dissipation during the Cenozoic and Late Cretaceous were weaker than at present, with the exception of the glacial states over the last 2 Ma. It is very likely that the Earth–Moon system is unusually dissipative at present. Consequently, the Moon's recession rate was slower in the deep past than predicted using PD dissipation rates, supporting the old-age Earth–Moon model. Furthermore, our relative dissipation rates in Fig. 4 support the lower range of dissipation values from Zeeden et al. (2014), who claim that the tidal dissipation between 11.5–12.3 Ma was either within 10% of PD values or 40% of the present rate. This has significant implications for climate proxy reconstructions: their lower estimate of the tidal dissipation rate was obtained by inserting a complete additional precession cycle, which our relative rates show is the correct dissipation rate to use. This highlights the importance of dynamic ellipticity in orbital chronology calculations, and it shows that accurate tidal dissipation rates must be used in investigations of palaeo-climates.

Acknowledgements

The tidal simulation output is available from the corresponding author. Funding was provided by the Natural Environmental Research Council (grants NE/F014821/1 and NE/I030224/1 to JAMG), and the National Science Foundation (grant 0927946-ATM to MH). Simulations were done using HPCWales, and technical support from Ade Fewings is gratefully acknowledged.

References

Arbic, B.K., Karsten, R.H., Garrett, C., 2009. On tidal resonance in the global ocean and the back-effect of coastal tides upon open-ocean tides. Atmos.-Ocean 47, 239–266.

Berger, A., Loutre, M., Laskar, J., 1992. Stability of the astronomical frequencies of the Earth's history for paleoclimate studies. Science 255, 560–566.

Bills, B., Ray, R., 1999. Lunar orbital evolution: a synthesis of recent results. Geophys. Res. Lett. 26, 3045–3048.

Canup, R., Asphaug, E., 2001. Origin of the Moon in a giant impact near the end of the Earth's formation. Nature 412, 708–712.

Coughenour, C., Archer, A., Lacovara, K., 2013. Calculating Earth–Moon system parameters from sub-yearly tidal deposit records: an example from the carboniferous tradewater formation. Sediment. Geol. 295, 67–76.

Darwin, G.H., 1899. The Tides and Kindred Phenomena in the Solar System. Houghton, Boston.

Domeier, M., 2016. Vegetation–climate interactions in the warm mid-Cretaceous. Gondwana Res. 36, 275–295.

Egbert, G.D., Bennet, A.F., Foreman, M.G.G., 1994. Topex/Poseidon tides estimated using a global inverse model. J. Geophys. Res. 99, 24821–24852.

Egbert, G.D., Bills, B.G., Ray, R.D., 2004. Numerical modeling of the global semidiurnal tide in the present day and in the last glacial maximum. J. Geophys. Res. 109, C03003. http://dx.doi.org/10.1029/2003JC001973.

Egbert, G.D., Erofeeva, S., 2002. Efficient inverse modeling of barotropic ocean tides. J. Atmos. Ocean. Technol. 19, 183–204.
Egbert, G.D., Ray, R.D., 2001. Estimates of M2 tidal energy dissipation from Topex/Poseidon altimeter data. J. Geophys. Res. 106, 22475–22502.
Falahat, S., Nycander, J., 2015. On the generation of bottom-trapped internal tides. J. Phys. Oceanogr. 42, 526–545.
Green, J.A.M., 2010. Ocean tides and resonance. Ocean Dyn. 60.
Green, J.A.M., Huber, M., 2013. Tidal dissipation in the early Eocene and implications for ocean mixing. Geophys. Res. Lett. 40. http://dx.doi.org/10.1002/grl.50510.
Hansen, K., 1982. Secular effects of oceanic tidal dissipation on the moons orbit and the Earth's rotation. Rev. Geophys. 20, 457–480.
Herold, N., Huber, M., Müller, R.D., Seton, M., 2012. Modeling the Miocene climatic optimum: ocean circulation. Paleoceanography 27, PA1209.
Husing, S., Hilgen, F., AbdulAziz, H., Krijgsman, W., 2007. Completing the Neogene geological time scale between 8.5 and 12.5 Ma. Earth Planet. Sci. Lett. 253, 340–358.
Jakobsson, M., Mayer, L.A., Coakley, B., Dowdeswell, J.A., Forbes, S., Fridman, B., Hodnesdal, H., Noormets, R., Pedersen, R., Rebesco, M., Schenke, H.-W., A, Y.Z., Accettella, D., Armstrong, A., Anderson, R.M., Bienhoff, P., Camerlenghi, A., Church, I., Edwards, M., Gardner, J.V., Hall, J.K., Hell, B., Hestvik, O.B., Kristoffersen, Y., Marcussen, C., Mohammad, R., Mosher, D., Nghiem, S.V., Pedrosa, M.T., Travaglini, P.G., Weatherall, P., 2012. The International Bathymetric Chart of the Arctic Ocean (IBCAO) Version 3.0. Geophys. Res. Lett. 29, L12609.
Kagan, B., Sundermann, A., 1996. Dissipation of tidal energy, paleotides, and evolution of the Earth–Moon system. Adv. Geophys. 38, 179–266.
Lambeck, K., 1980. The Earth's Variable Rotation: Geophysical Causes and Consequences. Cambridge University Press, Cambridge, UK.
Laskar, J., Robutel, P., Joutel, F., Correia, M.G.A., Levrard, B., 2004. A long-term numerical solution for the insolation quantities of the Earth. Astron. Astrophys. 428, 261–285.
Lourens, L., Brumsack, R.W.H., 2001. Geological constraints on tidal dissipation and dynamical ellipticity of the Earth over the past three million years. Nature 409, 1029–1033.
Lourens, L., et al., 2001. Astronomical pacing of late Palaeocene to early Eocene global warming events. Nature 7045, 1083–1087.
Matthews, K., Williams, S., Whittaker, J., Muller, R., Seton, M., Clarke, G., 2015. Geologic and kinematic constraints on Late Cretaceous to mid Eocene plate boundaries in the southwest Pacific. Earth-Sci. Rev. 140, 72–107.
Muller, R.D., Seton, M., Zahirovic, S., Williams, S.E., Matthews, K.J., Wright, N.M., Shephard, G.E., Maloney, K.T., Barnett-Moore, N., Hosseinpour, M., Bower, D.J., Cannon, J., 2016. Ocean basin evolution and global-scale plate reorganization events since Pangea breakup. Annu. Rev. Earth Planet. Sci. 44, 107–138.
Munk, W., 1966. Abyssal recipes. Deep-Sea Res. 13, 707–730.
Munk, W., 1968. Once again – tidal friction. Q. J. R. Astron. Soc. 9, 352–375.
Murray, C., Dermott, S., 2010. Solar System Dynamics. Cambridge University Press. 608 pp.
Ooe, M., 1989. Effects of configuration and bathymetry of the oceans on the tidal dissipation of the Earth's rotation. J. Phys. Earth 37, 345–355.
Padman, L., Fricker, H.A., Coleman, R., Howard, S., Erofeeva, S., 2002. A new tidal model for the Antarctic ice shelves and seas. Ann. Glaciol. 34, 247–254.
Palike, H., Shackleton, N., 2000. Constraints on astronomical parameters from the geological record for the last 25 Myr. Earth Planet. Sci. Lett. 182, 1–14.
Platzman, G.W., Curtis, G.A., Hansen, K.S., Slater, R.D., 1981. Normal modes of the world ocean 2. Description of modes in the periods range 8 to 80 hours. J. Phys. Oceanogr. 11, 579–603.
Poliakov, E., 2005. Numerical modelling of the paleotidal evolution of the Earth–Moon system. Dynamics of Populations of Planetary Systems 197, 445–452.
Poulsen, C.J., Zhou, J., 2013. Sensitivity of Arctic climate variability to mean state: insights from the Cretaceous. J. Climate 26, 7003–7022.
Schmittner, A., Green, J.A.M., Wilmes, S.-B., 2015. Glacial ocean overturning intensified by tidal mixing in a global circulation model. Geophys. Res. Lett. 42. http://dx.doi.org/10.1002/2015GL0635610.
Smith, W.H.F., Sandwell, D.T., 1997. Global seafloor topography from satellite altimetry and ship depth soundings. Science 277, 1957–1962.
Sonett, C., 1996. Late Proterozoic and Paleozoic tides, retreat of the Moon, and rotation of the Earth. Science 273, 100–104.
Walker, J., Zahnle, K., 1986. Lunar nodal tide and distance to the Moon during the Precambrian. Nature 320, 600–602.
Waltham, D., 2004. Anthropic selection for the Moon's mass. Astrobiology 4, 460–468.
Waltham, D., 2015. Milankovitch period uncertainties and their impact on cyclostratigraphy. J. Sediment. Res. 85, 990–998.
Webb, D., 1982. Tides and the evolution of the Earth–Moon system. Geophys. J. R. Astron. Soc. 70, 261–271.
Wells, M., Allison, P., Piggott, M., Hampson, G., Pain, C., Gorman, G., 2010. Tidal modeling of an ancient tide-dominated seaway, part 1: model validation and application to global early Cretaceous (Aptian) tides. J. Sediment. Res. 80, 393–410.
Williams, G., 2000. Geological constraints on the Precambrian history of Earth's rotation and the Moon's orbit. Rev. Geophys. 38, 37–59.
Williams, J., Turyshev, S., Boggs, D., 2014. The past and present Earth–Moon system: the speed of light stays steady as tides evolve. Planet. Sci. 3, 1–9.
Wilmes, S.-B., Green, J.A.M., 2014. The evolution of tides and tidally driven mixing over 21,000 years. J. Geophys. Res. 119. http://dx.doi.org/10.1002/2013JC009605.
Wunsch, C., Ferrari, R., 2004. Vertical mixing, energy, and the general circulation of the oceans. Annu. Rev. Fluid Mech. 36, 281–314. http://dx.doi.org/10.1146/annurev.fluid.36.050802.122121.
Zeeden, C., Hilgen, F., Hüsing, S., Lourens, L., 2014. The miocene astronomical time scale 9–12 Ma: new constraints on tidal dissipation and their implications for paleoclimatic investigations. Paleoceanography 29, 296–307.
Zhou, J., Poulsen, C., Rosenbloom, N., Shields, C., Briegleb, B., 2012. Vegetation-climate interactions in the warm mid-Cretaceous. Clim. Past 8, 565–576.